Felix Schuler, Sebastian Dany, Christoph John and Michael de Wild*

Exploitation of transition temperatures of NiTi-SMA by adjusting SLM parameters

Non-linear dependency of transition temperature on SLM manufacturing parameters

Abstract: It is well known that the transition temperatures, e.g. the austenite peak temperature A_p, of NiTi Shape Memory Alloys (SMAs) can be adjusted by changing the alloy composition. This topic recently became more interesting due to the possibilities to produce SMA-parts by additive manufacturing, specifically by Selective Laser Melting (SLM). The potential of new designs and smart structures by so-called *4D-printing* with locally adjusted transition temperatures A_p potentially opens up new applications and novel temperature-responsive medical devices. This work focuses on the SLM manufacturing parameters *exposure time ET* (scanning speed) and *laser power P* and their impact on the transition temperature A_p beyond the commonly used generic process parameter *energy density ED*. By systematical variation of process- and scan-parameters, the impact of the *P*, *ET*, sample orientation and *layer height LH* as well as interdependencies between them have been studied. A wide range of transition temperatures A_p between -20°C and 70°C has been reached from one starting material by varying *ET*. These findings potentially allow the manufacturing of smart devices with multi-stage deformation processes in a single 4D-printed part.

Keywords: Selective Laser Melting, NiTi, Transition Temperature.

https://doi.org/10.1515/cdbme-2021-2016

Felix Schuler: University of Applied Sciences Northwestern Switzerland FHNW, School of Life Sciences HLS, Institute for Medical Engineering and Medical Informatics IM², Hofackerstrasse 30, CH-4132 Muttenz, Switzerland
***Corresponding author: Michael de Wild**: University of Applied Sciences Northwestern Switzerland FHNW, School of Life Sciences HLS, Institute for Medical Engineering and Medical Informatics IM², Hofackerstrasse 30, CH-4132 Muttenz, Switzerland, michael.dewild@fhnw.ch
Sebastian Dany: University of Applied Sciences Northwestern Switzerland FHNW, School of Life Sciences HLS, Institute for Medical Engineering and Medical Informatics IM², Hofackerstrasse 30, CH-4132 Muttenz, Switzerland. Hochschule Hamm-Lippstadt, D-59063 Hamm, Germany
Christoph John: Department of Chemistry, University of Basel, Mattenstrasse 24a, CH-4058 Basel, Switzerland,

1 Introduction

It has been well established that the transition temperature A_p of NiTi based SMAs manufactured by SLM can be adjusted with increasing the *energy density ED* of the laser during the manufacturing process [1][2]. This change in transition temperature is primarily a consequence of the faster evaporation of nickel ($flux_{Ni} > flux_{Ti}$) during the SLM process (based on the Langmuir equation, see *figure 1*) and a resulting shift in composition of the resulting alloy [3][4].

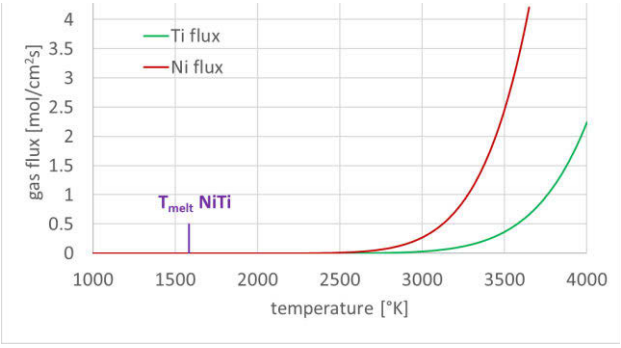

Figure 1: Calculated flux of matter from the melt pool for nickel and titanium based on the Langmuir equation and gas pressure data [3][4].

Recently, this phenomenon has been closer investigated by several researchers and it has been shown that *energy density ED* as a sole parameter is not sufficient to describe the phenomenon [5]. The individual parameters of the printing process like *laser power P*, *exposure time ET* (scanning speed) or *hatch design* have a specific impact on the transition temperature A_p and can be used to tune the properties in a controlled way [6][7]. This study additionally investigated the impact of other building parameters in the SLM process like the part orientation and the *layer height LH* and connects the observations with latest concepts.

To understand the impact of the individual manufacturing parameters it is paramount to understand the underlying melting, evaporation and solidification processes: In the SLM process, a powder bed is illuminated by a scanning laser, liquefies locally and creates a heat affected zone (HAZ) with a melt pool in the powder layer and underlying contact surface, following the lasers path and leaving behind a trace of

solidified melt track welded to the underlying substrate (*figure 2*).

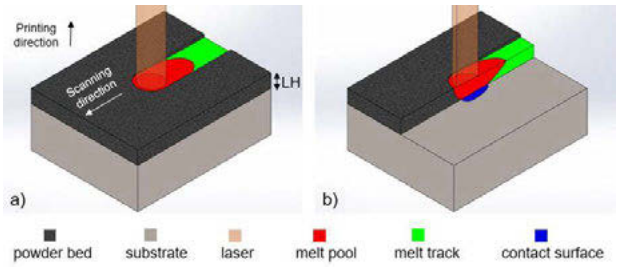

Figure 2: Schematic of the SLM process (a) and in cross section (b). The shape/size of the melt pool and the contact surface depend strongly on printing parameters and material properties. Different cooling rates influence the solidification and thus the final composition, microstructure and transition temperature A_p of the NiTi alloy.

During the local, short-term melting, excessive heating/cooling rates (>10^5 C/sec) and high temperatures occur well above the NiTi melting point of approx. 1580°K and material can even evaporate. As stated above, due to the element-specific flux rate, the evaporation rate of nickel is significantly above that of titanium, see *figure 1*. As a consequence, the relative composition of the melt pool will change. Therefore, the size and temperature of the melt pool and the *exposure time ET* are strongly correlated to the relative loss of nickel in the alloy and hence to the transition temperature A_p. Besides the printing parameters, also the thermal and structural connection to the underlying solid substrate, and material properties like thermal conductivity play a role in the resulting melt pool dimensions. It was found that materials with higher heat conductivity have smaller melt pools because the substrate can better act as a heat sink [8].

2 Material and methods

2.1 Sample design and analysis

The particle size distribution of the starting NiTi powder [9] was determined by laser diffraction (Helos, with dry disperser RODOS and vibratory feeder, Sympatec GmbH, Clausthal-Zellerfeld, Germany) and the particle morphology was characterized by Scanning Electron Microscope (SEM, Hitachi TM3030Plus). The pre-alloyed NiTi powder particles exhibit spherical morphology with a d_{50}-value of 57.2 ± 1.9 µm and an austenite peak temperature A_p = 9°C.
The samples were designed in SolidWorks™ 2019 CAD (*Dassault Systèmes, France*) and produced on a modified SLM machine (Realizer, DMG Mori, Germany). The sample geometry was a cylindrical disc of ø3 mm and height of 1.2 mm, adjusted to the sample container of the Differential Scanning Calorimeter (DSC 214 *Polyma* NETZSCH, -150°C to 150°C, 10 K/min). All samples were characterized by DSC and the peak of the austenite transformation temperature A_p was determined.

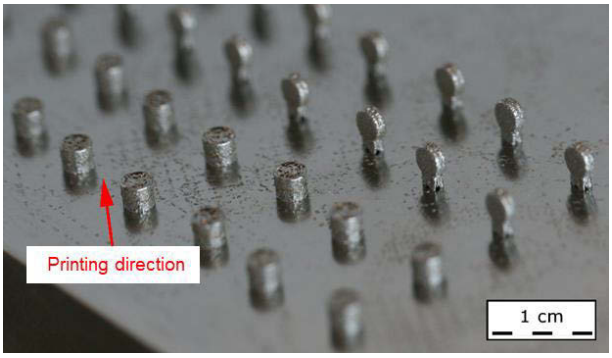

Figure 3: ø3 mm NiTi-disks on SLM-building platform in horizontal (along cylinder axis) and vertical (in radial) printing direction.

2.2 Investigated SLM parameter sets

The investigated parameter range for *laser power P* and *exposure time ET* are shown in *figure 4* for both *layer heights LH* 25 µm and 50 µm. A *laser current LC* 2500 mA corresponds to a *laser power P* 93.5 Watts and, with the *point distance PD* set to 30 µm, the *exposure time ET* 100 µs (resp. 200 µs for *LH* 50 µm) results in a scanning speed of 0.3 m/s (resp. 0.15 m/s for *LH* 50 µm). The used *hatch distance HD* was 80 µm. *Figure 4* shows the experimental parameter map for the *exposure time* (*ET* with constant *P*) and *laser power* (*P* with constant *ET*). As a reference point ("anchor"), the parameters from a previous study were used [10]. The generic process parameter *energy density ED* is defined as the introduced power per volume (1):

$$ED = \frac{P\ ET}{PD\ HD\ LH} \quad (1)$$

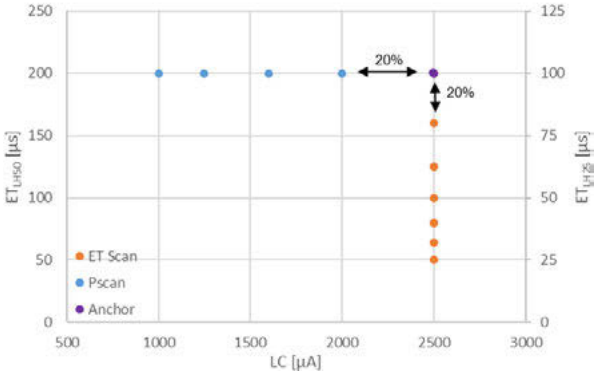

Figure 4: Parameter map of ET and LC for ø3 mm NiTi disk produced in two different layer heights LH: 25 µm and 50 µm.

Two different *LH* were investigated, corresponding to 25 µm and 50 µm powder layer thickness *LH*, keeping the energy density *ED* comparable by scaling *ET*. To investigate if the printing direction has an effect, the cylindrical samples were printed in a horizontal and vertical direction, see *figure* 3.

3 Results

Exemplary DSC data is shown in *figure 5* and *figure 6* to illustrate the transformation temperature A_p of the obtained material using different parameter sets in SLM manufacturing. As expected, they all show a shift to higher transition temperatures upon increased *energy density ED*.

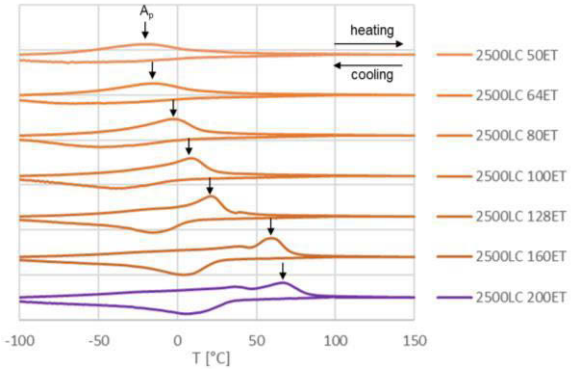

Figure 5: DSC data of the horizontal LH50 ET-scan (LC = const = 2500 µA).

The *ET*-scan (*figure 5*) shows a gradual shift of A_p from -21°C to +66°C and the change of the DSC profile is gradual. However, A_p in the *P*-scan (*figure 6*) seems to be barely affected until reaching the anchor parameter set with a sudden increase of A_p. This behavior was observed to different degrees in all investigated parameter sets, independent on orientation and *LH*.

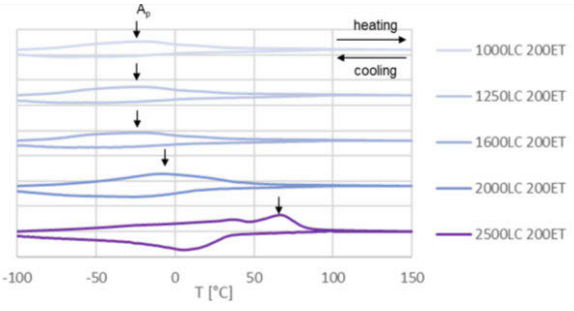

Figure 6: DSC data of the horizontal LH50 P-scan (ET = const = 200 µs).

The influence of the individual process parameter on A_p becomes apparent, when plotted against *ED* (*figure 7*). The general increase in A_p with higher *ED* is observable over all samples as well as the more linear increase of A_p in the *ET*-scan when compared to the *P*-scan.

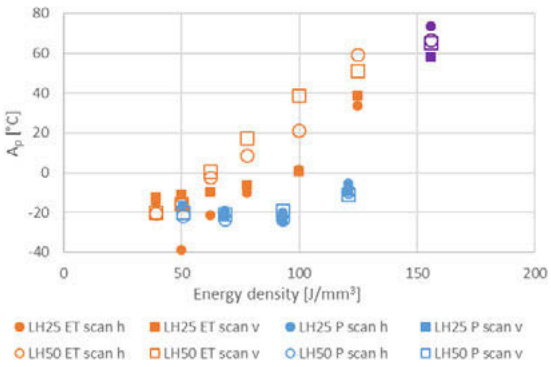

Figure 7: A_p for all samples as a function of the calculated energy density ED. ET-scan, P-scan, h: horizontal, v: vertical building direction. Open symbol: 50 µm LH, closed symbols: 25 µm LH.

Furthermore, it was observed, that the difference in A_p of the *ET*- and *P*-scans is more pronounced for thicker *LH* at comparable *ED* (compare *figure 7* open vs. closed markers. Overall, the influence on A_p is more prominent for vertically printed than for horizontally printed samples.

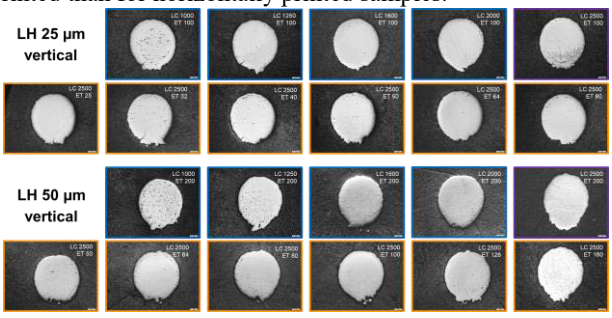

Figure 8: SEM cross-sections. Top: LH25 vertical, and Bottom: LH50 vertical disks produced by ET- and LC-scans.

The printability and material density are demonstrated in *figure 8* over the complete range of the investigated process window. A trend towards reduced porosity was observed for higher *ED*.

4 Discussion

As mentioned in the introduction, the change in A_p is primarily a consequence of the chemical composition, which is influenced by the element-specific flux out of the melt pool, i.e. preferential evaporation of Ni.

The gradual increase of A_p for the *ET*-scans can be understood by the increase of the *exposure time ET* which gives the material proportionally more time to evaporate from the melt pool. At a constant laser power *P (LC)*, a higher total flux of Ni is the consequence. A linear behavior is expected and therefore could be a promising approach for transition temperature adjustment.

The *P*-scan at constant *ET* on the other hand reveals an initially smaller change, in accordance to [10]. Only with higher laser power a significant change in A_p can be measured. This is most probably a consequence of the fact that the surface temperature of the melt pool is directly impacted by the laser power *P*. Because, as discussed earlier by Langmuir (see figure 1), the flux depends strongly on this temperature, it is assumed that A_p is primarily influenced at elevated *P* when the difference between Ni- and Ti-flux becomes significant.

Furthermore, we observed that thicker powder layers *LH* amplify this effect. It is assumed that this is a consequence of the pronounced insulation effect of the increased *LH* which leads to a smaller contact surface with the substrate and consequently to less heat loss towards the substrate (see *figure 2*). This reduces the cooling rate of the melt pool and increases its size. The increased surface and temperature could then be responsible for the amplified total flux and consequently the larger difference in A_p when compared to thinner *LH*. This assumption is also supported by meltpool simulations of Gusarov [8].

Although the printing direction was expected to have an impact on A_p, the results obtained are inconclusive. The thermal connectivity of the part to the substrate is weaker in vertical printing direction than in horizontal printing direction. In the latter case, the thermal energy can dissipate better to the substrate, which increases its capacity as a heatsink for the building process. Additionally, due to the increased print surface per layer in the horizontal samples, the laser settling time, i.e. the duration in-between layers are longer and the sample has more time to cool down. Therefore, A_p was expected to be less affected for horizontal samples. However, our experiments could not confirm this hypothesis.

As demonstrated in SEM cross-sections, the samples were successfully printed within the entire window of process parameters. However, an increased porosity was identified using low *laser power P* as well as geometric deviations on the underside of the parts.

5 Conclusions

It was shown that the shift of the composition and the transformation temperature A_p in printed NiTi SMA parts is not only dependent on *ED*. The situation is more complex and the individual parameters of the SLM process have to be considered when tuning the properties of additively manufactured NiTi devices. *ET* is a proper tool to precisely adjust local composition and consequently A_p of the SMA. The layer thickness *LH* and, to some extent, the printing direction seem to have a minor impact on the phase transformation temperature, not changing the general nature of the dependencies of A_p on *ET* and *P*. A proper parameter study to establish the process should therefore be sufficient to implement a process able to manufacture NiTi SMA parts with locally adjusted A_p.

Author Statement

Research funding: The SPIRITS project [11] is supported by the Region Grand Est, Land Baden-Württemberg, Land Rheinland-Pfalz, Cantons Baselstadt, Basellandschaft, Aargau, Swiss Confederation and by the program INTERREG Upper Rhine from the ERDF (European Regional Development Fund). Conflict of interest: Authors state no conflict of interest.

References

[1] M. de Wild, F. Meier, T. Bormann, C.B.C. Howald, B. Müller, *Damping of selective-laser-melted NiTi for medical implants*, Journal of Materials Engineering and Performance, **23**, 7; 2614-19 (2014).

[2] T. Bormann, B. Müller, M. Schinhammer, A. Kessler, P. Thalmann, M. de Wild, *Microstructure of selective laser melted nickel–titanium*, Materials Characterization, **94**, 189–202 (2014), doi: 10.1016/j.matchar.2014.05.017.

[3] C.B. Alcock, V.P. Itkin, M.K. Horrigan, *Vapour Pressure Equations for the Metallic Elements*: 298–2500K., Canadian Metallurgical Quarterly, **23**, No. 3, pp. 309-313, (1984).

[4] T. DebRoy, S.A. David, *Physical processes in fusion welding*. Rev. Mod. Phys., **67**, 85–112 (1995).

[5] W. Chen, Q. Yang, S. Huang, S. Huang, J. J. Kruzic, X. Li, *Laser power modulated microstructure evolution, phase transformation and mechanical properties in NiTi fabricated by laser powder bed fusion*, Journal of Alloys and Compounds, **861**, 157959, (2021), doi: 10.1016/j.jallcom.2020.157959.

[6] X. Wang, *et al. Effect of process parameters on the phase transformation behavior and tensile properties of NiTi shape memory alloys fabricated by selective laser melting*. Additive Manufacturing, **36**, 101545 (2020).

[7] Y. Yang *et al. Laser beam energy dependence of martensitic transformation in SLM fabricated NiTi shape memory alloy,* Materialia **6**, 100305 (2019).

[8] A.V. Gusarov, I. Smurov, *Modeling the interaction of laser radiation with powder bed at selective laser melting*. Physics Procedia, **5**, 381–394 (2010).

[9] SAES Getters S.p.A., Viale Italia 77, I-20020 Lainate (Milan), Italy, https://www.saesgetters.com/

[10] T. Bormann, B. Müller, M. Schinhammer, A. Kessler, P. Thalmann, M. de Wild, *Microstructure of selective laser melted nickel-titanium*, Materials Characterization, **94**, 189-202 (2014).

[11] INTERREG-project *Smart Printed Interactive Robots for Interventional Therapy and Surgery*, http://www.interreg-spirits.eu